Article:
Anstöter, Cate S., Wong, Natalie G.K., Selwe, Kgato P. et al. (2023) Laser Interfaced Mass Spectrometry of the Sunscreen Molecule Octocrylene Demonstrates that Protonation Does Not Impact Photostability. Chemphotochem. e202300133. ISSN: 2367-0932

https://doi.org/10.1002/cptc.202300133

ChemPhotoChem

Research Article
doi.org/10.1002/cptc.202300133

Chemistry Europe
European Chemical Societies Publishing

www.chemphotochem.org

Laser Interfaced Mass Spectrometry of the Sunscreen Molecule Octocrylene Demonstrates that Protonation Does Not Impact Photostability

Cate S. Anstöter,[a] Natalie G. K. Wong,[a] Kgato P. Selwe,[a] and Caroline E. H. Dessent*[a]

Octocrylene (OCR) is a widely used organic sunscreen molecules, and is a dominant component of many sunscreen formulations. Here, we perform the first measurements on the protonated form of OCR, *i.e.* $[OCR+H]^+$, to probe whether protonation affects the molecule's photostability. The novel photochemical technique of UV laser-interfaced mass spectrometry is employed from 400–216 nm, revealing that the electronic absorption spectrum of OCR across the S_1 and S_2 states red shift by 40 nm upon protonation. Our measurements reveal that $[OCR+H]^+$ predominantly undergoes photofragmentation into the *m/z* 250 and 232 ionic products, associated with loss of its bulky alkyl side chain, and subsequent loss of water, respectively. We compare the photochemical fragmentation results with higher-energy collisional dissociation results to investigate the nature of the photodynamics that occur following UV absorption. The excited state decay pathways over the S_1 and S_2 excited states of $[OCR+H]^+$ are associated with statistical fragmentation in line with dominant ultrafast decay. This behaviour mirrors that of neutral OCR, demonstrating that protonation does not affect the ultrafast decay pathways of this sunscreen molecule. We discuss our results in the context of the known breakdown of OCR into benzophenone, identifying a potential photoactivated pathway to benzophenone formation in solution.

Introduction

Sunscreens play an important role in human health since they reduce the risk of skin exposure to damaging ultraviolet solar radiation, and hence sunburn and skin cancer.[1–3] For organic sunscreen molecules, one of the primary active components of commercial sunscreens, their effectiveness is associated with their intrinsic ability to absorb UV photons, and the extent to which they are and remain photostable over time.[4] A sunscreen molecule that is photo-unstable over a relatively short timescale will be of limited use in a sunscreen formulation and could potentially degrade into reactive or toxic end products. It is therefore crucial to characterize the factors that affect the photostability of individual sunscreen molecules and determine the identity of any photoproducts.[5,6] Aside from the direct consequences to human health, information on photostability and photoproduct identity is important for assessing the impact of sunscreens in the natural environment, which is of timely societal concern since over 14,000 tons of sunscreen are believed to enter aquatic environments each year.[7–9] Indeed, for sunscreen molecules there is a tension between the desirability of long-timescale photostability and UV filtering, balanced against persistence in the natural environment and associated environmental risks.[10]

Mass spectrometry approaches have been used extensively for probing the photostability of sunscreens and assessing their photoproducts.[11,12] More recently, laser-interfaced mass spectrometry (LIMS) has been shown to be a valuable experimental method for probing the intrinsic UV absorption properties and photochemistry of organic sunscreen molecules.[13–16] It is particularly useful in the context of analysing photoproducts, since these can be straightforwardly identified by mass spectrometry following photoexcitation and decay of a precursor ion. In these experiments, the organic chromophore is introduced to the MS via electrospray ionization and studied either as the protonated or deprotonated form of the molecule,[17–19] or in a complex with an attached ion-tag, such as an alkali metal cation.[16] The ionic sunscreen precursor ion is isolated in an ion trap, where it is irradiated with photons across the UV range, and the photoproducts obtained at each photoexcitation energy measured. LIMS has been successfully applied over recent years to a range of organic sunscreen chromophores in their protonated, deprotonated and cation-metal complexed forms to better understand how pH and charge state affect the intrinsic photostability.[13]

In this work, we apply LIMS to probe the sunscreen Octocrylene (OCR: 2-Ethylhexyl-2-cyano-3,3-diphenylprop-2-enoate), investigating its intrinsic photochemistry and photodegradation pathways. The structure of OCR is illustrated in Scheme 1, and it is studied here in its protonated form, i.e. $[OCR+H]^+$, where protonation is expected to occur on the carbonyl group oxygen by analogy with similar systems. While the ester group will not display a high affinity for protons,

[a] Dr. C. S. Anstöter, Dr. N. G. K. Wong, K. P. Selwe, Prof. C. E. H. Dessent
Department of Chemistry
University of York
Heslington, YO10 5DD (UK)
E-mail: caroline.dessent@york.ac.uk

Supporting information for this article is available on the WWW under https://doi.org/10.1002/cptc.202300133

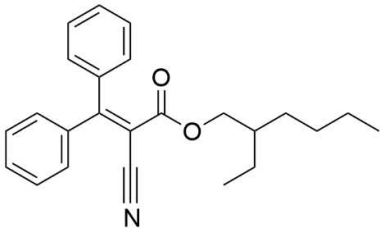

Scheme 1. Schematic diagram of octocrylene (OCR).

complexation with a proton can occur within the oily, complex environment of a sunscreen mixture,[2] making the measurements here of interest for optimisation of commercial sunscreens.[13] Higher energy collisional dissociation (HCD) measurements are presented alongside the LIMS photodissociation data, to aid the interpretation of the photodissociation mass spectra and provide insight into the system's photodynamics.[20] These complementary collisional and photoexcitation dissociation measurements allow us to identify photochemical products that are mediated by long-lived, dissociative excited state pathways.[18]

OCR is one of the most common UV filters used in commercial sunscreen products and is also present in other cosmetics such as moisturizers and lip balms.[21] It is one of only 14 UV filter molecules currently approved for use in over-the-counter products in the USA.[22] OCR primarily filters UVB radiation (280 nm–320 nm), with some activity over the UVA-II part of the spectrum (320 nm–340 nm). It is also used as a stabilizer of other components of a sunscreen mixture, such as the broad UVA absorber Avobenzone.[23] The identity of photoproducts produced from OCR is currently an issue of heightened importance, since recent studies have indicated that benzophenone may be a direct degradation product of OCR.[24] Benzophenone is associated with a wide range of toxicities, including genotoxicity, carcinogenicity and endocrine disruption.[24,25] Furthermore, OCR is rapidly becoming the dominant UV sunscreen environmental contaminant found in coastlines, rivers and lakes across the world,[26–28] leading to significant environmental concerns about the potential increase in benzophenone as a result. The LIMS measurements performed here allow us to probe whether a direct photochemical breakdown pathway exists for OCR that would enhance production of benzophenone.

Experimental Section

OCR (98% purity) was purchased from Sigma Aldrich and was used without further purification. HPLC-grade ethanol was purchased from Fisher Scientific, Inc. (Pittsburgh, PA, USA) and again used as received.

Laser-Interfaced Mass Spectrometry. The experiment has been described in-full previously.[29] Briefly, gas-phase UV photodissociation experiments were conducted in an AmaZon SL dual funnel electrospray ionization quadrupole ion trap (ESI-QIT) mass spectrometer (Bruker Daltonics Inc., Billerica, MA, USA), which was modified to allow for laser-interfaced mass spectrometry.[30] Solutions of OCR (1.0×10^{-4} mol dm^{-3} with trifluoroacetic acid to aid protonation) in EtOH were introduced to the mass spectrometer via ESI using typical instrumental parameters: nebulizing gas pressure of 10.0 psi, an injection rate of 0.33 mL/h, a drying gas flow rate of 8.0 L/min, and run in the positive ion mode at a capillary temperature of 160 °C to form the protonated species, $[OCR+H]^+$. Small amounts of trifluoroacetic acid were added to the OCR solution to enhance ionization efficiency.

$[OCR+H]^+$ ions were mass selected and isolated in the ion trap prior to UV laser irradiation. UV photons were produced with a 10 Hz Nd:YAG (Surelite™, Amplitude Laser Group, San Jose, CA, USA) pumped OPO laser (Horizon™, Amplitude Laser Group, San Jose, CA, USA), providing ~0.3 mJ across the range 400–216 nm (3.10–5.74 eV). Laser step sizes of 2 nm were used throughout. The laser beam was focused as described previously.[30] Photofragmentation experiments were conducted with a set ion accumulation time of 10 ms and a corresponding fragmentation time of 100 ms, allowing for each mass-selected ion packet to interact with one laser pulse and minimize the likelihood of multiphoton events. In the initialisation stage of measurements, the laser power was optimized to ensure that single photon conditions were present. This process is described in detail in Ref. [15]. When fluorescence is negligible, UV-excited gaseous ions fragment upon excited-state relaxation, yielding an action absorption spectrum by photodepletion.[30–32]

Analysis. In line with previous analysis,[29] the photodepletion (PD) of $[OCR+H]^+$ was measured as a function of scanned wavelength, with the photofragment production (PF) recorded simultaneously at each corresponding wavelength. As described by Equations (1) and (2), Int_{OFF} and Int_{ON} represent the parent ion intensities with laser off and on, respectively; Int_{FRAG} is the photofragment intensity with the laser on; λ is the excitation wavelength (nm); and P is the tuneable laser pulse energy (mJ).

$$\text{Photodepletion Intensity} = \frac{\ln\left(\frac{Int_{OFF}}{Int_{ON}}\right)}{\lambda \times P} \quad (1)$$

$$\text{Photofragment Production Intensity} = \frac{\ln\left(\frac{Int_{FRAG}}{Int_{OFF}}\right)}{\lambda \times P} \quad (2)$$

The photodepletion intensities were taken from an average of three repeat runs at each wavelength within the range studied. We note that photofragment ions with $m/z < 50$ are not detectable within our mass spectrometer since low masses fall outside of the mass window of the ion trap.

Higher-Energy Collisional Dissociation. Experiments were performed in a Thermo Fisher Orbitrap Fusion™ mass spectrometer, as described previously,[20] with the following settings: the syringe was operated at a flow rate of 3 μL/min and with the following settings: MS2 scan isolation mode, ion trap; detector type, ion trap; positive ion spray voltage (3500 V); RF lens (60%); normalized AGC target (100%); maximum injection time (100 ms); ion transfer tube temperature (275 °C); and vaporizer temperature (20 °C). For the MS scan in this instrument, the settings were as follows: detector type, Orbitrap; positive ion spray voltage (3200 V); RF lens (45%); normalized AGC target (100%); and maximum injection time (100 ms).

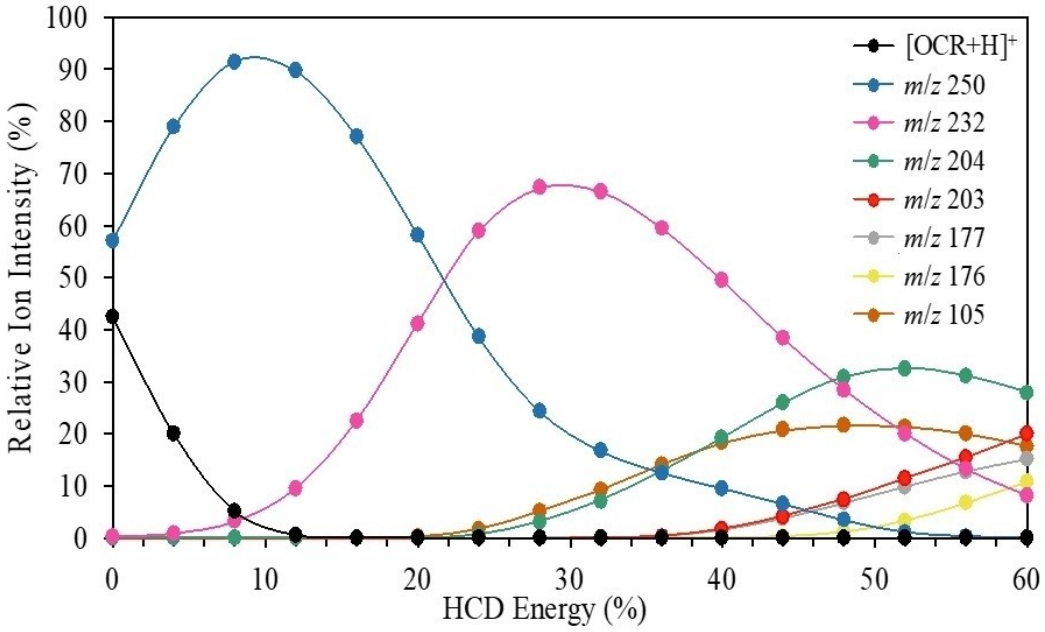

Figure 1. Percent ion intensity of the collision-induced fragments of $[OCR+H]^+$ (*m/z* 362) as a function of HCD energy. The solid line is a three-point adjacent average of the data points.

Results and Discussion

Higher-Energy Collisional Dissociation

To probe the identity of the fragments produced from a hot ground state, HCD was conducted on $[OCR+H]^+$. These measurements characterize the ground-state fragmentation pathways of the molecular ion as a function of increasing internal energy. It therefore allows the identification of secondary fragments, which can be formed from successive fragmentation of primary fragments at high internal energy.[20]

Figure 1 shows the HCD results for $[OCR+H]^+$, illustrating that the precursor ion readily dissociates with dominant fragmentation into the *m/z* 250 and *m/z* 232 fragment ions. Suggsted structures of the dominant fragments are shown in Scheme 2. The *m/z* 250 fragment can be assigned as arising from loss of the 2-ethlyhexyl alkyl side chain of OCR, with the *m/z* 232 fragment then being associated with loss of water from the protonated carbonyl group of *m/z* 250 (Table 1). The production profile of these fragments indicates that *m/z* 250 is produced at the lowest collisional energies but fragments with increasing cross section into *m/z* 232 as a function of increasing internal energy. This allows us to assign *m/z* 232 as a secondary fragment of *m/z* 250. Similarly, the production profiles of the *m/z* 204 and *m/z* 105 fragments indicate that they are secondary fragments of *m/z* 232, with the other minor fragments (*m/z* 176, 177 and 203) only increasing in intensity at the highest collisional energies. Table 1 lists the fragment ions observed, with tentative assignments of the relevant fragment identities (see Scheme 2).

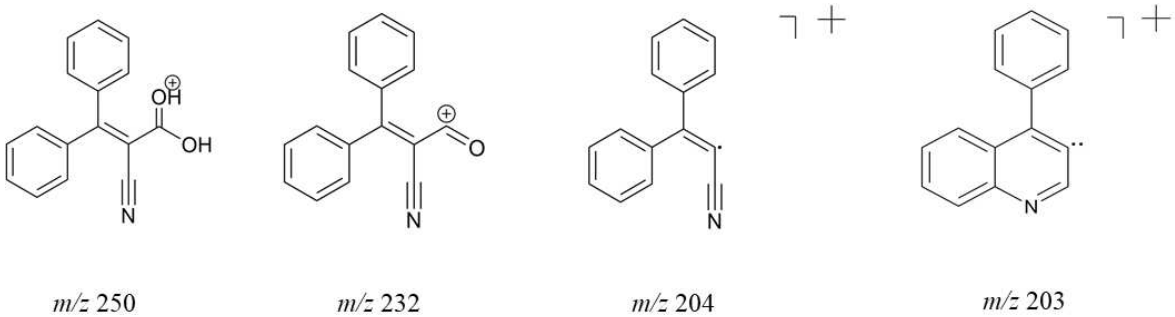

Scheme 2. Suggested structures of the major ionic fragments observed in LIMS and HCD of $[OCR+H]^+$.

Table 1. Summary of the major ionic and associated neutral fragments of $[OCR+H]^+$ (*m/z* 362) produced upon UV laser excitation (LIMS) and during HCD. Proposed structures of the major fragments are given in Scheme 2.

m/z	Formula of Ion	Formula of Neutral Loss	HCD	LIMS
250	$C_{16}H_{12}O_2N$	C_8H_{16}	✓	✓
232	$C_{16}H_{10}ON$	$C_8H_{18}O$	✓	✓
204	$C_{15}H_{10}N$	$C_9H_{18}O_2$	✓	✓
203	$C_{15}H_9N$	$C_9H_{19}O_2$	✓	✓
178	$C_{14}H_{10}$	$C_{10}H_{18}O_2N$	X	✓
177	$C_{14}H_9$	$C_{10}H_{19}O_2N$	✓	✓
176	$C_{14}H_8$	$C_{10}H_{20}O_2N$	✓	✓
105	C_7H_5O	$C_{17}H_{23}NO$	✓	✓

Gas-phase UV Absorption Spectrum (Photodepletion Spectrum) of $[OCR+H]^+$

The photodepletion (gas-phase absorption) spectrum of mass-selected $[OCR+H]^+$ across the 3.10–5.74 eV (400–216 nm) range is shown in Figure 2(a). Mass selection is a key advantage of the experimental approach as it allows us to directly probe the intrinsic properties of the protonated form of OCR, which is not straightforward in the solution phase.

The gaseous absorption spectrum of $[OCR+H]^+$ displays strong absorption in the UV–A region (with an onset below the lowest measured photon energy of 3.1 eV) through Band **I**, and also through a second region of strong absorption (Band **II**) which lies within the UV–B (3.6–4.2 eV). Absorption again increases above $h\nu = 4.5$ eV into the UV–C wavelength region (**III**). The solution-phase UV absorption spectrum of neutral OCR has been recorded previously and shows a broad, intense absorption which peaks around $h\nu = 300$ nm, in methanol and cyclohexane.[33] Figure 2(a) shows that the gas-phase absorption spectrum of $[OCR+H]^+$ is red shifted by ~40 nm compared to the solution phase neutral (non-protonated) system.

TD-DFT calculations (Section S1) were performed on both the neutral and protonated forms of OCR, solvated and unsolvated, to investigate whether the red shift arises largely as a result of solvation or protonation. Protonation is expected to occur at the central carbonyl group, in line with similar systems,[15,17,34] and was found to introduce only very minor changes to both the geometric structure and the ordering and character of the frontier orbitals (Section S2). However, we note that even these subtle changes lead to several differences between the neutral and protonated molecules' UV-Vis spectra. Namely, we note the significant red-shift in the UV-Vis spectrum of $[OCR+H]^+$ and the change in density of states beneath Band I between the protonated and neutral OCR spectra. The calculations indicate that the red-shift is, in part, associated with the perturbation of the chromophore upon protonation of the electronically conjugated carbonyl group. Similar absorption red-shifts have been observed for protonation of other conjugated systems.[35,36] Further consideration of the optically bright excited states indicate a change in character of the dominant transitions between the two systems (Section S2). For

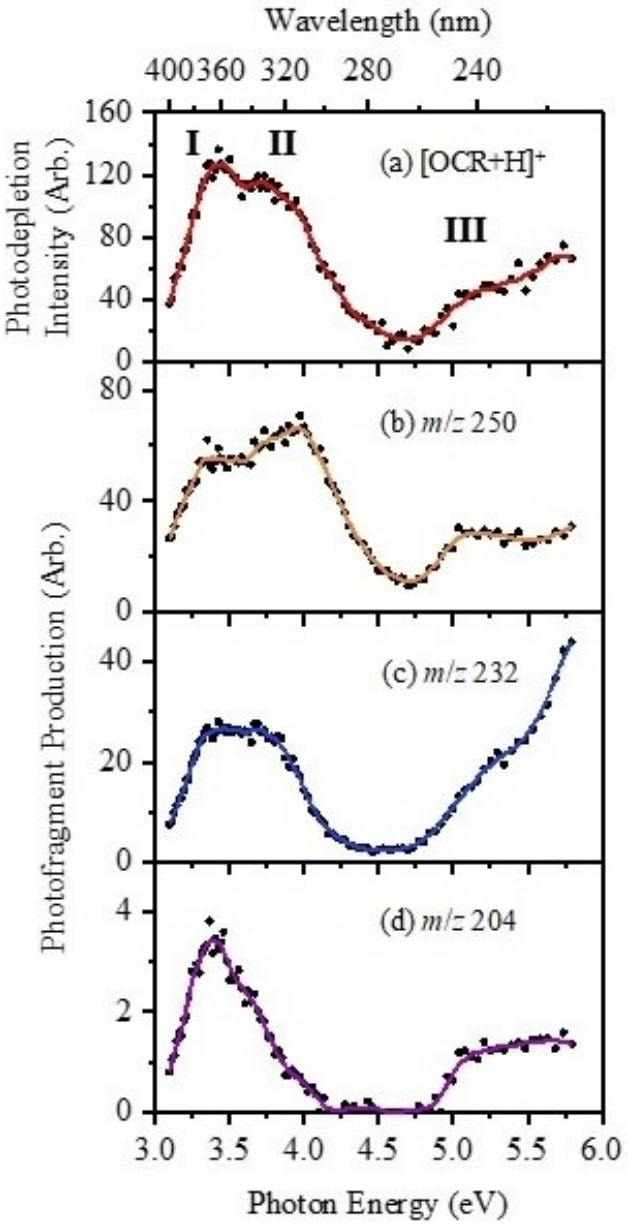

Figure 2. (a) Gas-phase UV absorption (photodepletion) spectrum of $[OCR+H]^+$ and photofragment production spectra of the three major photofragments (b) *m/z* 250, (c) *m/z* 232, and (d) *m/z* 204. The solid line is a five-point adjacent average of the data points.

OCR the transition with the highest oscillator strength is the $^1 1\pi\pi^*$ (HOMO to LUMO), while for $[OCR+H]^+$ the $^1 3\pi\pi^*$ (HOMO-2 to LUMO) state has the highest oscillator strength. The transition defining the latter state can be considered as having increased charge-transfer character, contributing to the red-shift of the spectra, in agreement with previous findings in the literature.[37,38]

The TD-DFT calculations of $[OCR+H]^+$ predict two strong electronic transitions, HOMO→LUMO (3.36 eV) and HOMO-2→LUMO (3.43 eV) (Figure S3), which likely correspond to the Band **I** and Band **II** features (Figure 2(a)), and align with the previously identified S_1 and S_2 excited states of neutral OCR.[39]

Photofragmentation of $[OCR+H]^+$

To gain further insight into the excited-state decay dynamics, and the nature of the photodecay products, we next inspect the photofragment production spectra. Figure 2(b)–(d) display the production spectra of the most intense fragment ions. The *m/z* 250 photofragment (Figure 2(b)) is the most intense fragment ion, with its production profile following the Band **I** and Band **II** absorption features across the UVA/UVB region. The production intensity is slightly higher for the UVB Band **II** than for the UVA Band **I**. This *m/z* 250 fragment is also produced through the UVC region of Band **III**, with a relatively flat spectral profile. The second most intense photofragment is *m/z* 232, is produced with similar intensity through Bands **I** and **II**, but with intensity rising strongly through Band **III**. The HCD results presented in Figure 1 show that the *m/z* 250 ion fragments with loss of H_2O at higher internal energies, consistent with the increased production of *m/z* 232 at higher photoexcitation energies. The third most intense photofragment is *m/z* 204. Intriguingly, this photofragment displays a profile that is distinct from both the *m/z* 250 and *m/z* 232 photofragments, with production largely associated with Band **I** excitation, and falling production through the Band **II** region. Like the *m/z* 250 photofragment, its intensity is flat through the Band **III** region, revealing that it is not being produced through fragmentation of *m/z* 232.

The intensities of the more minor photofragments (Figure 3) of $[OCR+H]^+$ are significantly lower than those of the major photofragments, particularly so compared to the very dominant *m/z* 250 and *m/z* 232 photofragments. The production profiles of these minor photofragments are generally similar to those of the major photofragments, with production over the Band **I**, **II** and **III** regions. Comparing the photofragments to the HCD fragments of $[OCR+H]^+$ (Figure 1), all of the major fragments appear as HCD fragments, with only *m/z* 178 from the minor photofragments not being produced via HCD, and hence being identifiable as a photochemical fragment. We note that this photofragment has a distinctive production profile, indicating that it does not arise from the same excited-state decay pathways. Table 1 summarises both sets of fragmentation results.

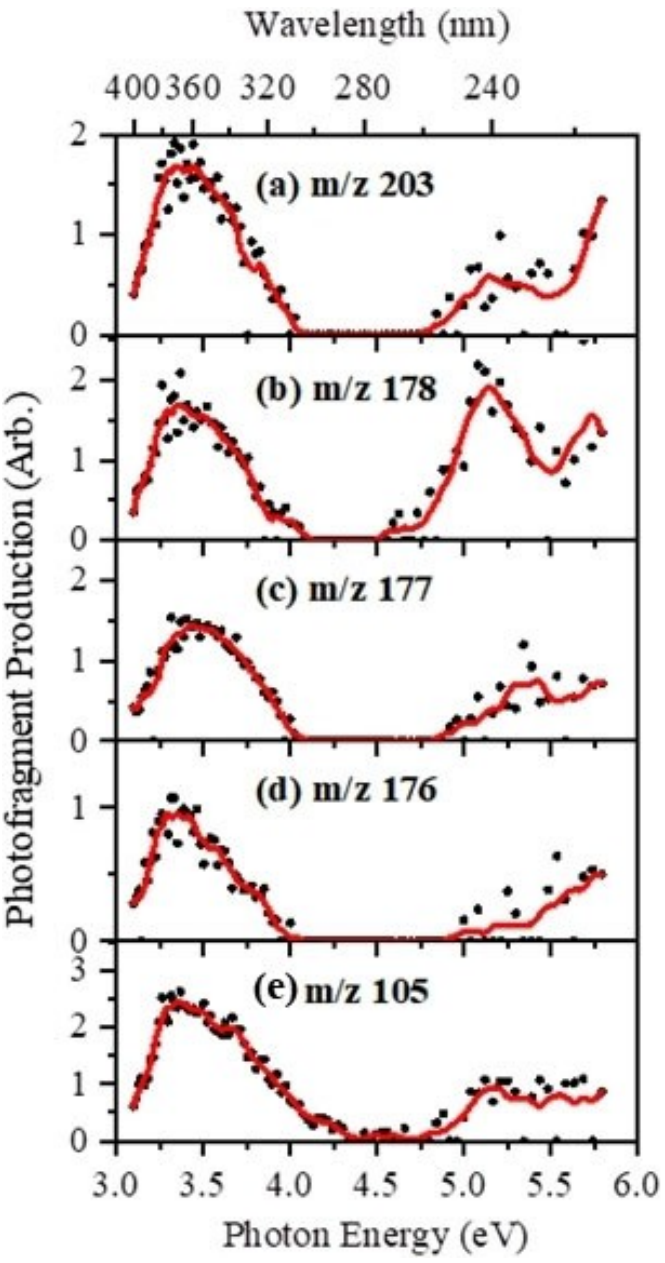

Figure 3. Photofragmentation action spectra of the minor fragments of $[OCR+H]^+$: (a) *m/z* 203, (b) *m/z* 178, (c) *m/z* 177, (d) *m/z* 176, and (e) *m/z* 105. The solid line is a five-point adjacent average of the data points.

Interpretation of the fragmentation patterns of $[OCR+H]^+$

To perform as an efficient UV filter, a molecule must be able to convert the harmful UV radiation it has absorbed into benign thermal energy.[4,13] This is achieved by electronic excited state(s) rapidly relaxing back to the electronic ground state from where excess energy can be dissipated by heat loss. In solution, this thermal energy can be transferred to the bulk solvent *via* vibrational relaxation, but in the gas phase, energy is conserved within the molecular system so that a hot ground state will dissociate across the available fragmentation pathways. These are the same as those available to the isolated molecule when it is heated, so called "statistical fragmentation".[40,41] For molecular ions, a closely comparable "heating" process occurs in collisional dissociation. If a molecular system is fragmenting *via* statistical fragmentation, the relative intensities of the various photofragments should mirror those found from HCD,[14,20] with the caveat that at high collision energies, secondary fragments can be produced from primary fragments.

For $[OCR+H]^+$ the major photofragments (Figure 2(b)–(d)) do match the major HCD fragments (Figure 1), indicating that the excited states accessed across the photoexcitation region studied here are largely decaying by statistical fragmentation. However, it is notable that the relative intensities of the major photofragments do vary with respect to one another across the Band **I**, **II** and **III** regions. Focusing on the UVA/UVB region that

is critical for sunscreen performance, the major fragment *m/z* 250 displays enhanced production over the Band **II** region (compared to the overall photodepletion profile), with the minor photofragment *m/z* 204 displaying enhanced production over Band **I**. These differences are likely associated with minor (longer lived) decay channels being accessed in the regions of Bands **I** (for *m/z* 204) and **II** (for *m/z* 250), respectively.

Further Discussion

OCR is widely viewed to be a high-performance UV filter molecule, with recent ultrafast laser spectroscopy measurements supporting this by identifying the intrinsic ability of OCR to rapidly dissipate UV photoexcitation.[33] The detailed excited-state decay pathways involved in UV dissipation by OCR have been investigated theoretically by Chang et al. who used computational methods to explore the potential energy surfaces and relaxation pathways of methyl 2-cyano-3,3-diphenylacrylate (MCDPA), a truncated chromophore of neutral OCR.[39] This combined QM/MM study provided insight into the known photodynamics, assigning the important excited states and identifying several efficient relaxation pathways that allow photoexcited MCDPA to repopulate the ground electronic state. The $\pi\pi^*$ TDDFT states calculated in this work (Section S1) are in good qualitative agreement with this high-level study, in terms of the nature of the molecular orbitals involved.

Our results show protonation does not affect the key decay pathways of OCR since the dominant relaxation pathways of $[OCR+H]^+$ are statistical decay pathways, in line with predominantly ultrafast decay.[14,40,41] This is strikingly different from other UV filters we have studied, for example oxybenzone and octyl-methoxycinnamate,[17,42] where protonation severely disrupts the UV energy dissipation pathways of the molecule. For OCR, our calculations predict that protonation entails only very limited geometric changes, and crucially, protonation does not block the molecular distortion associated with accessing the conical intersections that enable non-radiative relaxation to the ground electronic state.[43]

One point of note from the work of Chang *et al.* is that triplet states are believed to play a role in the decay dynamics of OCR, with the S_2 excited state believed to evolve through a T_2 state, to the T_1 state prior to relaxing to S_0.[39] Such longer-lived triplet states are frequently associated with dissociative photochemistry, and formation of photoproducts.[18,44–46] Notably, we observe enhanced production of the major fragment, *m/z* 250, in the region above the S_2 state (Band **II**), suggesting that longer-lived triplet states may be facilitating excited-state dissociation of $[OCR+H]^+$ into *m/z* 250 in this region.

Sunscreen molecules are increasingly detected globally in freshwater and marine environments, leading to concerns for the environmental impact of both primary sunscreens and also their breakdown products.[24–26] As noted in the introduction, OCR is rapidly becoming the dominant sunscreen contaminant in aquatic environments and knowledge of its photoproducts is therefore important in assessing its overall environmental impact. Photolysis measurements on OCR have found that 3–3-diphenylacrylonitrile is a significant photoproduct, matching our observation of the *m/z* 204 photofragment here.[47] Since 3–3-diphenylacrylonitrile was observed alongside benzophenone in the solution-phase photolysis measurements, it raises questions as to whether the breakdown of OCR into toxic benzophenone is being enhanced by a photochemical pathway via initial photoproduction of 3–3-diphenylacrylonitrile followed by hydrolysis and breakdown to benzophenone. It will be possible to investigate this in future experiments employing on-line mass spectrometry photolysis.[48] The gas-phase photodissociation results presented herein, alongside such on-line solution-phase measurements, should provide a clearer understanding of the route by which OCR breaks down to benzophenone.

Conclusions

In summary, we report for the first time the gaseous electronic photoabsorption spectrum and direct photofragment production profile spectra of the protonated form of OCR, a popular FDA-approved UVB filter found within many existing commercial sunscreens. The novelty of our gas-phase experiment is that it allows us to probe the direct impact of protonation on the effectiveness of OCR as a sunscreen molecule. We find that protonated OCR is able to dissipate UV energy via ultrafast decay in a similar manner to neutral OCR, so that protonation does not disrupt the UV filter activity for this molecule, unlike other common sunscreen molecules (e.g. avobenzone, oxybenzone) that we have studied previously.[15,17]

Acknowledgements

This work was funded through the Leverhulme Trust Research Project Grant RPG-2017-147. We thank the University of York and the Department of Chemistry for provision of funds for the OPO laser system. The York Centre of Excellence in Mass Spectrometry, used for the CID work, was created thanks to a major capital investment through Science City York, supported by Yorkshire Forward with funds from the Northern Way Initiative, and has more recently received additional support from the EPSRC and BBSRC. We also thank Mathew Hawkridge and Edward Matthews for their early contributions to this work.

Conflict of Interests

The authors declare no conflict of interest.

Data Availability Statement

The data that support the findings of this study are available from the corresponding author upon reasonable request.

Keywords: Sunscreens · octocrylene · mass spectrometry · lasers · photodegradation · photoproducts

[1] R. S. Mason, J. Reichrath, *Anti-Cancer Agents Med. Chem.* **2013**, *13*, 83–97.
[2] S. Forestier, *Journal of the American Academy of Dermatology* **2008**, *58*, S133–S138.
[3] U. Osterwalder, M. Sohn, B. Herzog, *Photodermatol. Photoimmunol. Photomed.* **2014**, *30*, 62–80.
[4] R. Losantos, I. Funes-Ardoiz, J. Aguilera, E. Herrera-Ceballos, C. García-Iriepa, P. J. Campos, D. Sampedro, *Angew. Chem. Int. Ed.* **2017**, *56*, 2632–2635.
[5] M. T. Ignasiak, C. Houée-Levin, G. Kciuk, B. Marciniak, T. Pedzinski, *ChemPhysChem* **2015**, *16*, 628–633.
[6] C. Stiefel, W. Schwack, Y.-T. H. Nguyen, *Photochem. Photobiol.* **2015**, *91*, 84–91.
[7] S. L. Schneider, H. W. Lim, *Journal of the American Academy of Dermatology* **2019**, *80*, 266–271.
[8] Y. S. D. Watkins, J. B. Sallach, *Integr. Environ. Assess. Manage.* **2021**, *17*, 967–981.
[9] C. L. Mitchelmore, K. He, M. Gonsior, E. Hain, A. Heyes, C. Clark, R. Younger, P. Schmitt-Kopplin, A. Feerick, A. Conway, L. Blaney, *Sci. Total Environ.* **2019**, *670*, 398–410.
[10] J. Labille, R. Catalano, D. Slomberg, S. Motellier, A. Pinsino, P. Hennebert, C. Santaella, V. Bartolomei, *Front. Environ. Sci.* **2020**, *8*, 101.
[11] J. Kockler, M. Oelgemöller, S. Robertson, B. D. Glass, *Journal of Photochemistry and Photobiology C: Photochemistry Reviews* **2012**, *13*, 91–110.
[12] Y.-T. Cho, H. Su, I.-C. Huang, C.-Y. Lai, Y.-D. Tsai, *Anal. Methods* **2019**, *11*, 6013–6022.
[13] N. G. K. Wong, C. E. H. Dessent, *Front. Chem.* **2022**, *9*, 812098.
[14] N. G. K. Wong, C. D. Rankine, C. E. H. Dessent, *J. Phys. Chem. Lett.* **2021**, *12*, 2831–2836.
[15] J. A. Berenbeim, N. G. K. Wong, M. C. R. Cockett, G. Berden, J. Oomens, A. M. Rijs, C. E. H. Dessent, *J. Phys. Chem. A* **2020**, *124*, 2919–2930.
[16] J. A. Berenbeim, N. G. K. Wong, M. C. R. Cockett, G. Berden, J. Oomens, A. M. Rijs, C. E. H. Dessent, *Phys. Chem. Chem. Phys.* **2020**, *22*, 19522–19531.
[17] N. G. K. Wong, J. A. Berenbeim, M. Hawkridge, E. Matthews, C. E. H. Dessent, *Phys. Chem. Chem. Phys.* **2019**, *21*, 14311–14321.
[18] N. G. K. Wong, J. A. Berenbeim, C. E. H. Dessent, *ChemPhotoChem* **2019**, *3*, 1231–1237.
[19] N. G. K. Wong, C. D. Rankine, C. S. Anstöter, C. E. H. Dessent, *Phys. Chem. Chem. Phys.* **2022**, *24*, 17068–17076.
[20] R. Cercola, E. Matthews, C. E. H. Dessent, *J. Phys. Chem. B* **2017**, *121*, 5553–5561.
[21] T. Maier, H. C. Korting, *Skin Pharmacol. Physiol.* **2005**, *18*, 253–262.
[22] National Drug Code Directory Database on March 8, **2019**, https://www.accessdata.fda.gov/scripts/cder/ndc/index.cfm.
[23] A. C. Kerr, *Clin. Exp. Dermatol.* **2011**, *36*, 541–543.
[24] C. A. Downs, J. C. DiNardo, D. Stien, A. M. S. Rodrigues, P. Lebaron, *Chem. Res. Toxicol.* **2021**, *34*, 1046–1054.
[25] *Natl Toxicol Program Tech Rep Ser* **2006**, 1–264.
[26] S. Ramos, V. Homem, A. Alves, L. Santos, *Sci. Total Environ.* **2015**, *526*, 278–311.
[27] C. A. Downs, M. S. Diaz-Cruz, W. T. White, M. Rice, L. Jim, C. Punihaole, M. Dant, K. Gautam, C. M. Woodley, K. O. Walsh, J. Perry, E. M. Downs, L. Bishop, A. Garg, K. King, T. Paltin, E. B. McKinley, A. I. Beers, S. Anbumani, J. Bagshaw, *J. Hazard. Mater.* **2022**, *438*, 129546.
[28] M. Carve, D. Nugegoda, G. Allinson, J. Shimeta, *Environ. Pollut.* **2021**, *268*, 115894.
[29] E. Matthews, *Photodissociation Spectroscopy of Gaseous Bio-Ions in a Commercial Quadrupole Ion Trap Mass Spectrometer*, University of York, **2018** (available online).
[30] E. Matthews, A. Sen, N. Yoshikawa, E. Bergström, C. E. H. Dessent, *Phys. Chem. Chem. Phys.* **2016**, *18*, 15143–15152.
[31] H. Yao, R. A. Jockusch, *J. Phys. Chem. A* **2013**, *117*, 1351–1359.
[32] R. Antoine, P. Dugourd, *Phys. Chem. Chem. Phys.* **2011**, *13*, 16494–16509.
[33] L. A. Baker, M. D. Horbury, V. G. Stavros, *Opt. Express* **2016**, *24*, 10700.
[34] E. Matthews, C. E. H. Dessent, *J. Phys. Chem. A* **2016**, *120*, 9209–9216.
[35] P. Nitschke, B. Jarząbek, A.-E. Bejan, M.-D. Damaceanu, *J. Phys. Chem. B* **2021**, *125*, 8588–8600.
[36] M. Trampuž, M. Žnidarič, F. Gallou, Z. Časar, *ACS Omega* **2023**, *8*, 1154–1167.
[37] Y. Toker, J. Langeland, E. Gruber, C. Kjær, S. B. Nielsen, L. H. Andersen, V. A. Borin, I. Schapiro, *Phys. Rev. A* **2018**, *98*, 043428.
[38] Y.-H. He, F.-M. Xie, H.-Z. Li, K. Zhang, Y. Shen, F. Ding, C.-Y. Wang, Y.-Q. Li, J.-X. Tang, *Mater. Chem. Front.* **2023**, *7*, 2454–2463.
[39] X.-P. Chang, Y.-G. Fang, G. Cui, *J. Phys. Chem. A* **2019**, *123*, 8823–8831.
[40] S. B. Nielsen, J. U. Andersen, J. S. Forster, P. Hvelplund, B. Liu, U. V. Pedersen, S. Tomita, *Phys. Rev. Lett.* **2003**, *91*, 048302.
[41] B. Lucas, M. Barat, J. A. Fayeton, C. Jouvet, P. Çarçabal, G. Grégoire, *Chem. Phys.* **2008**, *347*, 324–330.
[42] N. G. K. Wong, M. Sereli, C. S. Anstöter, C. E. H. Dessent, *Molecules* **2022**, *27*, 8796.
[43] L. A. Baker, B. Marchetti, T. N. V. Karsili, V. G. Stavros, M. N. R. Ashfold, *Chem. Soc. Rev.* **2017**, *46*, 3770–3791.
[44] L. Freitag, L. González, *J. Phys. Chem. Lett.* **2021**, *12*, 4876–4881.
[45] A. O. Lykhin, D. G. Truhlar, L. Gagliardi, *J. Am. Chem. Soc.* **2021**, *143*, 5878–5889.
[46] C. T.-L. Chan, C. Ma, R. C.-T. Chan, H.-M. Ou, H.-X. Xie, A. K.-W. Wong, M.-L. Wang, W.-M. Kwok, *Phys. Chem. Chem. Phys.* **2020**, *22*, 8006–8020.
[47] I. Karlsson, E. Persson, J. Mårtensson, A. Börje, *Photochem. Photobiol.* **2012**, *88*, 904–912.
[48] R. Cercola, N. G. K. Wong, C. Rhodes, L. Olijnyk, N. S. Mistry, L. M. Hall, J. A. Berenbeim, J. M. Lynam, C. E. H. Dessent, *RSC Adv.* **2021**, *11*, 19500–19507.

Manuscript received: June 25, 2023
Revised manuscript received: July 29, 2023
Accepted manuscript online: August 22, 2023
Version of record online: ■■, ■■

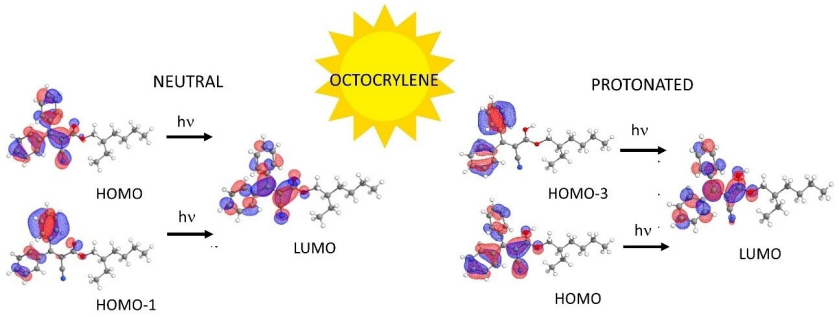

*Dr. C. S. Anstöter, Dr. N. G. K. Wong, K. P. Selwe, Prof. C. E. H. Dessent**

1 – 8

Laser Interfaced Mass Spectrometry of the Sunscreen Molecule Octocrylene Demonstrates that Protonation Does Not Impact Photostability

Laser photodissociation spectroscopy has been used to characterize the extent to which protonation affects the ability of octocrylene to act as an effective UV sunscreen molecule. We find that protonation results in a significant red shift of the absorption profile compared to non-protonated octocrylene, but does not impact on the ultrafast excited state decay pathways.